


Cite this: *RSC Adv.*, 2017, 7, 48437Received 29th August 2017
Accepted 26th September 2017

DOI: 10.1039/c7ra09567h

rsc.li/rsc-advances

The effects of He clusters on the mechanical properties of Ti_3AC_2 (A = Ge, Si): first-principles studies

Quan Song,^{ab} Peng Zhang,^{ab} Jun Zhuang^c and Xi-Jing Ning^{ab} 

Herein, the damage to the mechanical properties of Ti_3AC_2 (A = Ge, Si) was systematically investigated by first-principles calculations. It is known that the interstitial He atoms homogeneously generated in the materials would finally migrate to the A layer and form clusters of no more than 7 He atoms at a mono-vacancy in the A layer, and the cluster of 7 He atoms reduces the ideal tensile strength of Ti_3SiC_2 (or Ti_3GeC_2) to about 37.3% (or 35.5%). The strain simulations showed that the fracture would mostly occur around the A layer and enhances with increase in the cluster size, while the Ti_3C_2 blocks are relatively stable during tension. Although the He damage to the mechanical properties shows the similar trend for Ti_3SiC_2 and Ti_3GeC_2 , the former displays better properties for applications in nuclear structural devices.

1. Introduction

In general, He atoms are continuously generated in nuclear structural materials from (n, α) transmutation reactions and have a strong tendency to form He bubbles, leading to creep, swelling, embrittlement, or hardening of the materials.^{1–3} This He damage has been a problem in metals used as nuclear structural materials,^{1,4,5} recently, MAX phase materials (e.g. Ti_3SiC_2 and Ti_3AlC_2) have been considered as better candidates for nuclear structural materials^{6–9} and some experiments have demonstrated that Ti_3AlC_2 exhibits high tolerance to the He damage.^{10–12} For example, Wang *et al.* reported that Ti_3AlC_2 irradiated by 50 keV He ions with doses up to $1 \times 10^{18} \text{ cm}^{-2}$ at room temperature displayed severe structural disorder but no evident amorphization.¹¹ Patel *et al.* demonstrated that the Al layer of Ti_3AlC_2 at 500 °C irradiated by 200 keV He ions with doses of $2 \times 10^{17} \text{ cm}^{-2}$ was disordered, whereas the Ti_3C_2 layers remained intact after irradiation.¹² The previous theoretical studies of the MAX phase materials particularly focus on the single He atom behaviors, such as the energetically favorable interstitial sites for a single He atom to occupy and relevant effects.^{8,13–15} It should be noted that previous experimental observations showed that the He atoms implanted in MAX phase materials usually form clusters with sizes of 0.6–1.0 nm.^{10,11} Recently, we investigated the migration and aggregation of He atoms homogeneously generated in Ti_3SiC_2 *via* first-principles calculations¹⁶ and showed that the He atoms

would migrate to the Si layer and finally form clusters. Clearly, it is very important for the design of structural materials to study the effects of He clusters, instead of the single He atom, on the mechanical properties of Ti_3SiC_2 as well as other MAX phase materials.

In the present study, we mainly focus on the mechanical properties of Ti_3AC_2 (A = Ge, Si) affected by the He clusters *via* DFT calculations. First, we investigated the migration and segregation of He atoms homogeneously generated in Ti_3GeC_2 . It showed that interstitial He atoms would diffuse to the Ge layer at high temperature (>500 °C) and form clusters of no more than 7 He atoms by a single Ge vacancy, which is similar to the behavior of helium in Ti_3SiC_2 . Then, we examined the structural changes of Ti_3AC_2 in the presence of He clusters on stretching the materials and calculated the corresponding tensile stress. The results indicated that the ideal tensile strength of Ti_3SiC_2 (or Ti_3GeC_2) containing a cluster of 7 He atoms, which were formed at a vacancy in the A layer, reduces to 37.27% (or 35.47%) of the perfect ones. The structural deformation mainly takes place near the A layer, while the structure of the Ti_3C_2 block changes slightly.

2. Computational methods

The general chemical formula of MAX phase materials is $\text{M}_{n+1}\text{AX}_n$ with $n = 1, 2$, or 3, where M, A and X represent an early transition metal, the elements in group IIIA or IVA, and either carbon or nitrogen, respectively. The atoms are nano-layered arranged, as shown in Fig. 1 for Ti_3AC_2 , which can be regarded as a 'zigzag' stacking of hexagonal Ti_3C_2 blocks and planar A atomic sheets in the [0001] direction (z-axis) sequentially. This nano-laminated structure indicates that cleavage takes place mainly along the z-axis, which has been verified in some

^aInstitute of Modern Physics, Fudan University, Shanghai 200433, China. E-mail: xjning@fudan.edu.cn

^bApplied Ion Beam Physics Laboratory, Fudan University, Shanghai 200433, China

^cDepartment of Optical Science and Engineering, Fudan University, Shanghai 200433, China



experimental observations.^{17–19} Therefore, our examinations of the mechanical properties are restricted to the strain along the [0001] direction. Specifically, a uniaxial tensile strain ε was applied to the system along the [0001] direction step-by-step with an interval of 0.01. In each step, the system was allowed to be fully relaxed except fixing the z -axis to obtain the total energy E , which was employed to obtain ideal tensile stress:

$$\sigma = \frac{1}{V_0} \frac{\partial E}{\partial \varepsilon}, \quad (1)$$

where V_0 is the original volume of the system. This procedure continues until the tension σ reaches a maximum value σ_M , which is defined as ideal tensile strength; the corresponding strain ε_M is an important parameter for design of structural materials.

The cleavage of Ti_3AC_2 could take place around the A/Ti_{II}, Ti_{II}/C, or C/Ti_I interface, and we calculated the cleavage energy defined as:

$$E_{\text{cl}}(d) = (E_{\text{sep}} - E_{\text{whole}})/2S, \quad (2)$$

where E_{whole} is the total energy of a piece of Ti_3AC_2 with or without the presence of He clusters, and E_{sep} is the total energy of two departed parts, separated by d and cleaved from the materials between the A/Ti_{II}, Ti_{II}/C, or C/Ti_I interlayer, and S is the area of the interfaces.

To describe the behavior of He in Ti_3AC_2 , the solution energy is defined as follows:

$$E_{\text{He}}^s = E(\text{per} + \text{He}) - E(\text{per}) - E(\text{He}_{\text{iso}}), \quad (3)$$

where $E(\text{per} + \text{He})$ and $E(\text{per})$ are the total energies of Ti_3AC_2 with and without an interstitial He atom, respectively, and

$E(\text{He}_{\text{iso}})$ the energy of an isolated He atom. The formation energy of a vacancy of species X (X can be Ti, A or C) in Ti_3AC_2 is defined as:

$$E_{\text{V}_X}^f = E(\text{V}_X) - E(\text{per}) + \mu_X, \quad (4)$$

where $E(\text{V}_X)$ is the total energy of the system containing defect X, and μ_X denotes the corresponding chemical potential of the element.

A vacancy in Ti_3AC_2 could trap more than one He atom. In order to estimate the number of He atoms that could be adsorbed by a mono-vacancy, we define trapping energy by the following equation:^{20,21}

$$E_{\text{trap}} = E(\text{per} + n\text{He}, \text{V}) - E(\text{per} + (n-1)\text{He}, \text{V}) - E_{\text{He}}^s, \quad (5)$$

where $E(\text{per} + n\text{He}, \text{V})$ is the energy of Ti_3AC_2 with $n\text{He}$ atoms and a single vacancy, and E_{He}^s is the lowest solution energy determined by eqn (3). The maximum number of He atoms trapped by a single vacancy is determined when $E_{\text{trap}} > 0$.

The first-principles calculations were performed using density functional theory (DFT) and the pseudopotential plane-wave method implemented in the VASP codes, where a gradient-corrected form of the exchange correlation functional generalized gradient approximation (GGA-PW91) was employed.^{22,23} The cutoff energy of the plane-wave basis was set at 500 eV, and a $3 \times 3 \times 1$ supercell containing 108 atoms was adopted to perform the calculations, where $5 \times 5 \times 2$ Monkhorst-Pack k -point sampling for the Brillouin zone was chosen.²⁴ The lattice constants and internal freedom of the unit cell were fully optimized when atomic forces were less than $0.01 \text{ eV } \text{\AA}^{-1}$. The climbing image NEB method was employed to obtain the minimum energy path of the He atom.²⁵ Five images between the initial and final configurations were constructed by linear interpolation. The forces on all atoms in each image of the CI-NEB chain were converged to $0.05 \text{ eV } \text{\AA}^{-1}$. The tensile simulations were performed on a $2 \times 2 \times 1$ supercell, where $9 \times 9 \times 4$ k -points were generated, and the convergence of the total energy was $5.0 \times 10^{-5} \text{ eV}$ per atom.

3. Results and discussions

The migration and clustering of He atoms in Ti_3SiC_2 have been investigated in our recent study.¹⁶ It is shown that the He atoms that are homogeneously generated will quickly migrate into the Si layer at high temperature ($>500^\circ\text{C}$) and form clusters of no more than 7 He atoms at a mono-vacancy. The same procedures were performed to examine the behaviours of He atoms homogeneously generated in Ti_3GeC_2 .

According to eqn (3), the solution energy of He in I_{tetra1} , I_{tetra2} , I_{oct} , and I_{hex1} sites labelled by 1 (or 2), 3, 4 (or 5), and 6 in Fig. 2a are 5.07, 4.25, 3.16, and 3.59 eV, respectively, which are very close to the ones for Ti_3SiC_2 .¹⁶ The interlayer migration paths (Fig. 2a) and the corresponding energy barriers (Fig. 2b) are also similar to the ones of Ti_3SiC_2 , indicating that a He atom generated in Ti_3GeC_2 (or Ti_3SiC_2) at I_{tetra1} has to overcome an energy barrier of 1.045 eV (or 1.05 eV) jumping into the I_{oct} site near the Ge (or Si) layer. According to Arrhenius law, the period

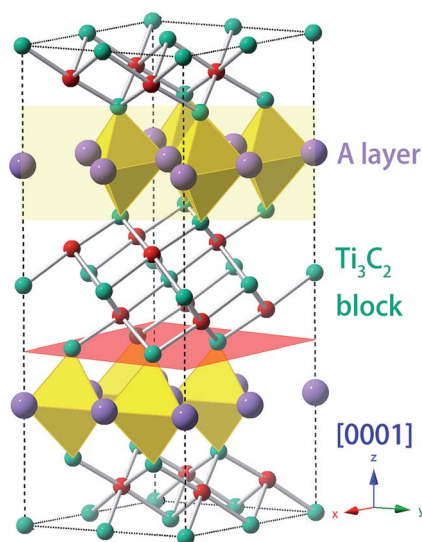


Fig. 1 Layered crystal structure of Ti_3AC_2 is divided into planar A atomic sheets and Ti_3C_2 blocks stacking in sequence along the z -axis in the [0001] direction. There are three total possible combination types of upper and lower surfaces, A/Ti_{II}, Ti_{II}/C, and C/Ti_I in Ti_3AC_2 phases. The green, red, and purple balls represent Ti, C, and A atoms, respectively.



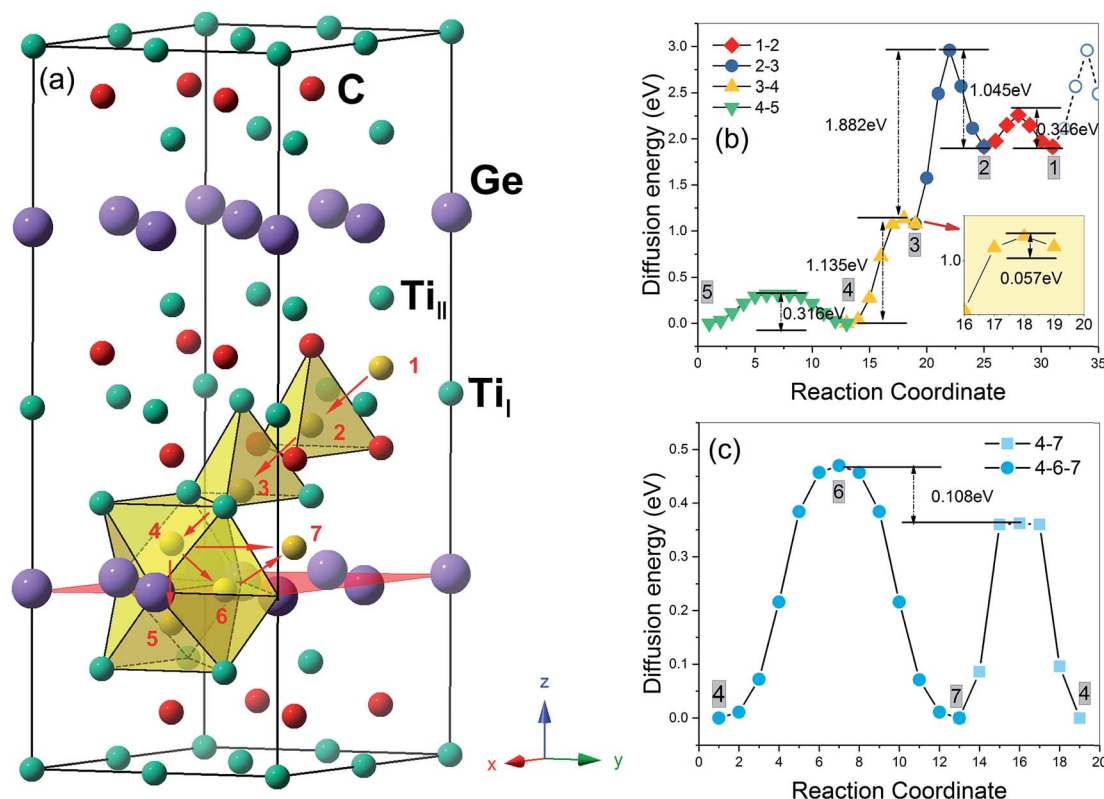


Fig. 2 Possible interstitial sites for a He atom to stay in Ti_3GeC_2 labelled by 1 (or 2), 3, 4 (or 5), 6 for $I_{\text{tetra}1}$, $I_{\text{tetra}2}$, I_{oct} , $I_{\text{hex}1}$, respectively (a); the diffusion barriers for a He atom migrating along the z-axis: $I_{\text{tetra}1}-I_{\text{tetra}1}$ (1–2), $I_{\text{tetra}1}-I_{\text{tetra}2}$ (2–3), $I_{\text{tetra}2}-I_{\text{oct}}$ (3–4), $I_{\text{oct}}-I_{\text{oct}}$ (4–5) (b); and the diffusion barriers between $I_{\text{oct}}-I_{\text{oct}}$ (4–7) and $I_{\text{oct}}-I_{\text{hex}1}-I_{\text{oct}}$ (4–6–7) along the Ge layer (c). The yellow balls represent He atoms.

for the He atoms staying at $I_{\text{tetra}1}$ is about 10 hours for room temperature (~ 300 K) and reduces to $\sim 10^{-6}$ s for the temperature of 800 K. The He atoms generated at the $I_{\text{tetra}2}$ site will quickly diffuse into the I_{oct} site near the Ge (or Si) layer due to the small diffusion barrier. Accordingly, all the interstitial He atoms generated homogeneously in Ti_3AC_2 at temperatures

above 500 °C will diffuse quickly into the A layer instead of staying in the other layers. For the diffusion of an He atom in the A layer, there exist two possible paths, $I_{\text{oct}}-I_{\text{oct}}$ (4–7) and $I_{\text{oct}}-I_{\text{hex}1}-I_{\text{oct}}$ (4–6–7), and the diffusion barrier of 0.36 eV along $I_{\text{oct}}-I_{\text{oct}}$ is lower than $I_{\text{oct}}-I_{\text{hex}1}-I_{\text{oct}}$ by 0.106 eV (Fig. 2c). However, it is significantly larger than the value (0.05 eV) in Ti_3SiC_2 , indicating that the mobility of He atoms in Ti_3GeC_2 along the A layer is much lower than that of Ti_3SiC_2 .

It should be pointed out that vacancies could be introduced in any layer of MAX phase materials by long-term nuclear irradiation and can trap the interstitial He atoms to form He clusters. For each cluster size, we attempted various possible patterns of He clusters to choose the most energy favorable one. According to eqn (4), the formation energies of a mono-vacancy (V) in the A, C, Ti_I , Ti_{II} layer of Ti_3GeC_2 (or Ti_3SiC_2) are 1.98 (or 1.95), 2.33 (or 2.16), 6.85 (or 7.18), and 4.58 (or 4.99) eV, respectively, showing that vacancy most easily forms in the A layer. According to eqn (5), the calculated trapping energy as the function of number of the He atoms trapped in a mono-vacancy in the Ge layer (Fig. 3) shows that the vacancy can trap no more than 7 He atoms, which is the same as that in the Si layer of Ti_3SiC_2 . The lattice constant changes of Ti_3GeC_2 induced by V- $n\text{He}$ clusters ($n = 0, 1, \dots, 7$) are similar to the changes of Ti_3SiC_2 . For the vacancy trapping fewer than 4 He atoms, the z-axis contracts, while the x-axis expands by about 0.5%, and with the

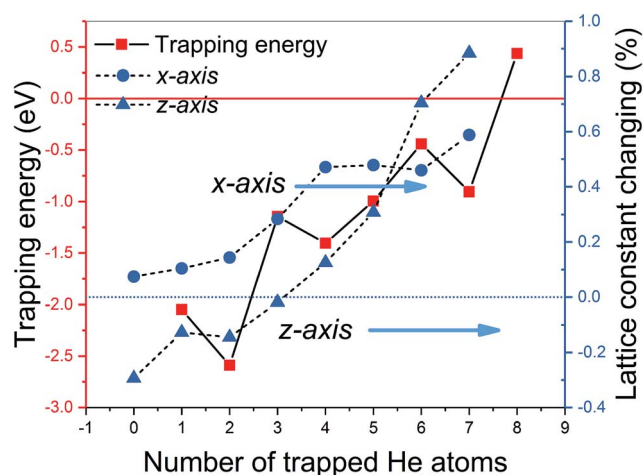


Fig. 3 The trapping energy (left y-axis) defined by eqn (5) and the corresponding lattice constant changing (right y-axis) with the number of He atoms trapped by a Ge mono-vacancy.

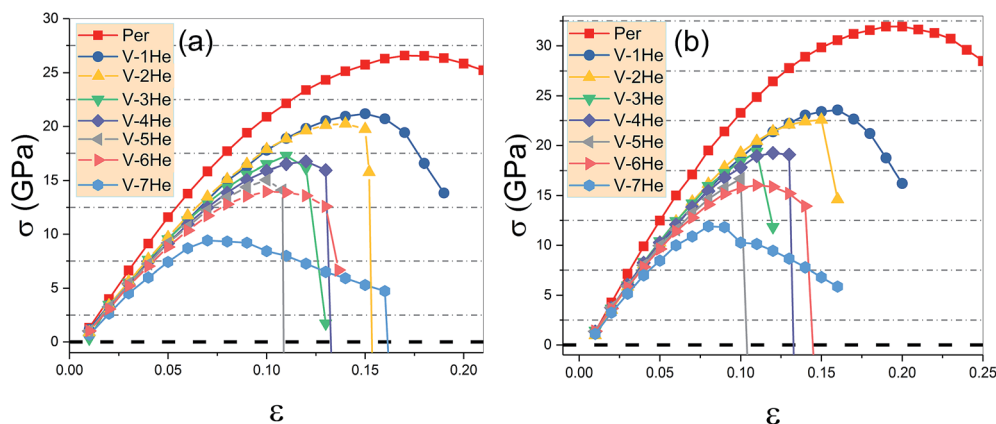


Fig. 4 The ideal tensile stress as the function of strain ε in the [0001] direction in the presence of V- n He ($n = 0, 1 \dots 7$) for Ti_3GeC_2 (a) and Ti_3SiC_2 (b).

Table 1 The ideal tensile strength σ_M of Ti_3AC_2 ($A = \text{Ge, Si}$) with V- n He clusters ($n = 0, 1 \dots 7$)

	σ_M (GPa)							
	Per	1He	2He	3He	4He	5He	6He	7He
Ti_3GeC_2	26.56	21.19	20.86	17.27	16.75	15.05	13.96	9.42
Ti_3SiC_2	31.93	23.57	22.59	19.38	19.24	16.70	16.04	11.90

increase in the He atoms, both the x - and z -axes expand by 0.6% and 0.9%, respectively.

As shown in Fig. 4, the ideal tensile strengths σ_M of perfect Ti_3SiC_2 and Ti_3GeC_2 are 31.93 GPa and 26.56 GPa, respectively, and the corresponding strains ε_M are 0.19 and 0.17, suggesting that Ti_3SiC_2 has better mechanical properties than Ti_3GeC_2 . With presence of the He cluster formed by a mono-vacancy in the A layer, the mechanical strength is significantly degraded as the size of the cluster increases as summarized in Table 1. For example, in the presence of a V-1He cluster, the σ_M of Ti_3SiC_2 (or Ti_3GeC_2) reduces to 23.57 GPa (or 21.19 GPa), which is about 73.8% (or 79.8%) of the values for the perfect materials; meanwhile, the corresponding ε_M decreases to 0.16 (or 0.15), and in the presence of a V-7He cluster, the σ_M and ε_M of Ti_3SiC_2 (or Ti_3GeC_2) reduce to 11.90 GPa (or 9.42 GPa) and 0.08 (or 0.07), which are about 37.3% (or 35.5%) and 42.1% (41.2%) of the perfect ones. Clearly, the presence of V- n He clusters ($n = 1, 2 \dots 7$) strengthens the embrittlement.^{26–28}

In the presence of He clusters trapped by a mono-vacancy in the A layer, the distances of A/ Ti_{II} , Ti_{II} /C, and C/ Ti_{I} interlayers denoted by d_1 , d_2 and d_3 under strain in the [0001] direction were examined. As shown in Fig. 5, the V- n He clusters ($n = 1, 2 \dots 7$) result in swelling of the A/ Ti_{II} interlayer and contracting of the Ti_{II} /C interlayer, while the C/ Ti_{I} interlayer remains nearly unchanged; the swelling is about ten times higher than the contracting (Fig. 5a1 and b1). For the materials without strain, d_1 of Ti_3SiC_2 (or Ti_3GeC_2) increases from 2.03 to 2.41 Å (or 2.10 to 2.45 Å) as the He atoms increase from 1 to 7; meanwhile, d_2 of Ti_3SiC_2 (or Ti_3GeC_2) decreases from 1.11 to 1.05 Å (or 1.09 to 1.03 Å). With the increase of the strain, the change in d_1 is

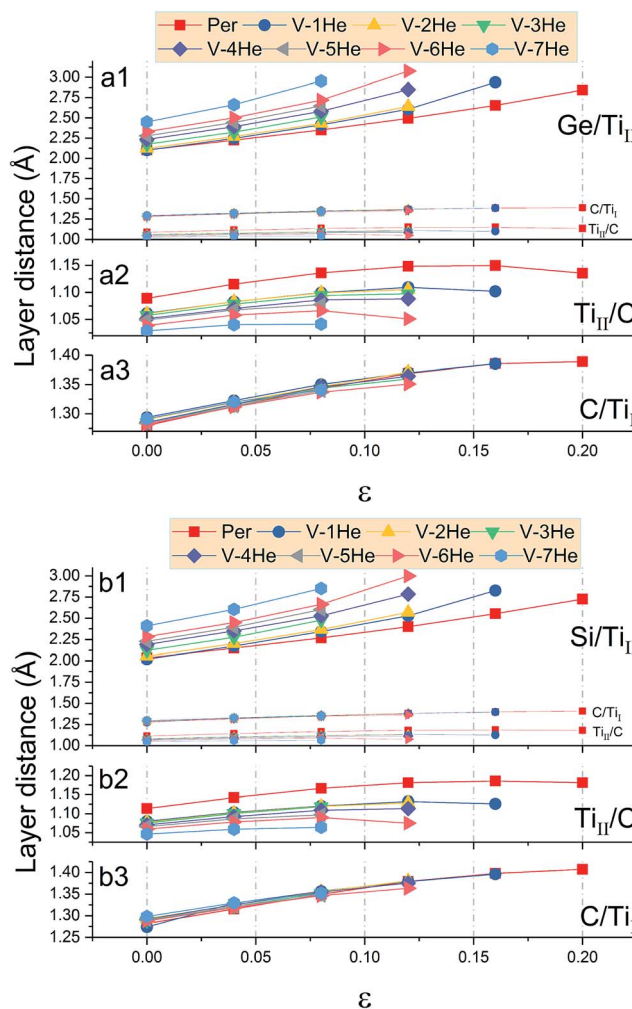


Fig. 5 The distances between A/ Ti_{II} , Ti_{II} /C, and C/ Ti_{I} interlayers as the function of strain ε for Ti_3GeC_2 (a1) and Ti_3SiC_2 (b1) with the presence of V- n He clusters ($n = 0, 1 \dots 7$) existing in the A layer. For clarity, the distances of Ti_{II} /C and C/ Ti_{I} interlayers are magnified in (a2, a3) and (b2, b3), respectively.



Table 2 The maximum strain ϵ_M of Ti_3AC_2 (A = Ge, Si) with V- n He clusters ($n = 1, 2, \dots, 7$) and the corresponding strain of each A/ Ti_{II} , Ti_{II} /C, and C/ Ti_{I} interlayer

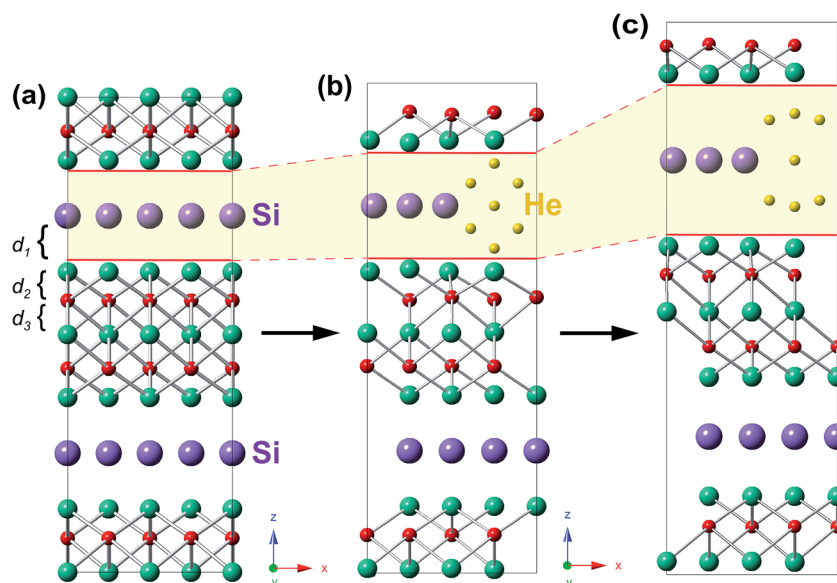
Block	Layer	Per	1He	2He	3He	4He	5He	6He	7He
Ti_3GeC_2 (ϵ)									
Ti_3Ge	Bulk	0.17	0.15	0.14	0.11	0.12	0.1	0.1	0.07
	Ge/ Ti_{II}	0.2832	0.3421	0.3221	0.2374	0.2757	0.2209	0.2417	0.1675
	Ti_{II} /C	0.0536	0.0434	0.0378	0.0407	0.0349	0.0260	0.0204	0.0146
Ti_3C_2	C/ Ti_{I}	0.0830	0.0708	0.0700	0.0585	0.0614	0.0509	0.0494	0.0344
Ti_3SiC_2 (ϵ)									
Ti_3Si	Bulk	0.19	0.16	0.15	0.11	0.12	0.1	0.11	0.08
	Si/ Ti_{II}	0.3183	0.3997	0.3531	0.3017	0.2710	0.2306	0.2678	0.1835
	Ti_{II} /C	0.0629	0.0423	0.0380	0.0418	0.0400	0.0298	0.0228	0.0169
Ti_3C_2	C/ Ti_{I}	0.0977	0.0959	0.0804	0.0652	0.0647	0.0525	0.0559	0.0413

significantly faster than that in d_2 . For example, in the presence of a V-7He cluster, when the strain reaches the maximum value ϵ_M , 0.08 for Ti_3SiC_2 (or 0.07 for Ti_3GeC_2), d_1 of Ti_3SiC_2 (or Ti_3GeC_2) changes from 2.41 to 2.85 Å (or 2.45 to 2.86 Å), increasing by about 18.35% (or 16.75%), while d_2 changes from 1.05 to 1.06 Å (or 1.03 to 1.04 Å), increasing by only 1.69% (or 1.46%). Under the maximum strain ϵ_M for V- n He clusters ($n = 1, 2, \dots, 7$) existing in the A layer, the strain of each interlayer is listed in Table 2. The results show that strain of the A/ Ti_{II} interlayer is much larger than that of the others, and the differences become larger with the increase in cluster size. On further increasing the strain, fracture took place around the A layer. Fig. 6a and b show the structural changes of perfect Ti_3SiC_2 caused by the presence of a V-7He cluster without strain. When this system was stretched to its maximum strain by 8%, the distance between the A/ Ti_{II} interlayer containing a V-7He cluster increases by about 18.35%, while the distance between other A/ Ti_{II} interlayers without the cluster remains nearly unchanged (Fig. 6c).

For Ti_3GeC_2 , similar structural changes were also observed, showing heavy damage effects of the cluster on the bond energy.

It is notable that both the Ti_{II} /C and C/ Ti_{I} interlayers are within the Ti_3C_2 blocks, so the above simulation results suggest that Ti_3C_2 blocks contribute more to the mechanical strength and structural stability. These results are consistent with the experimental observations that A layer is easily disordered, while the Ti_3C_2 structure appeared unperturbed after irradiation.^{9,12}

The above results suggest that the fracture of Ti_3AC_2 would mostly occur between the A/ Ti_{II} interlayer, which can be understood as follows. First, the MAX phases have the stacking sequence $\dots/[\text{M}-\text{X}]/\text{A}/[\text{M}-\text{X}]/\dots$ in the $[0001]$ direction with a characteristic 'zigzag' mode, and the bonds inside $[\text{M}-\text{X}]$ blocks are relatively stronger than those between the A layer and $[\text{M}-\text{X}]$ blocks.^{29–31} Second, the presence of He clusters in the A layer severely reduces the strength of the Ti-A bonds, which can be seen from the maximum cleavage energy, G_c ,

**Fig. 6** The optimized structure of perfect Ti_3SiC_2 (a) and the structure with a V-7He cluster existing in one of the Si layers without strain (b), which changes Ti_3SiC_2 with the presence of a V-7He cluster to (c) when the system was stretched by 8% to its maximum strain.

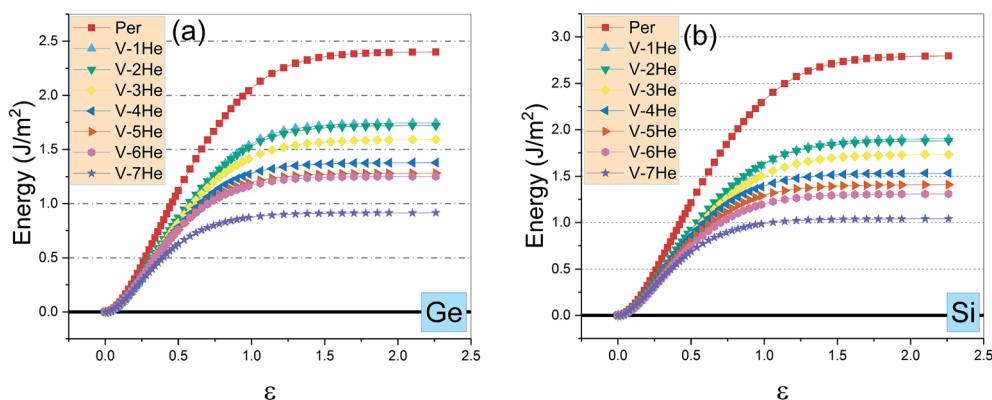


Fig. 7 The cleavage energy E_{cl} as the function of strain ϵ of the A/Ti_{II} interlayer in the presence of V-*n*He clusters (*n* = 1, 2...7) for Ti₃GeC₂ (a) and (b) Ti₃SiC₂.

which is the saturated value of $E_{cl}(d)$ when the distance d reaches infinity (cf. eqn (2)). As shown in Fig. 7, for the cleavage energy as the function of the strain ϵ of the A/Ti_{II} interlayer, the calculated G_c for Ti₃SiC₂ (or Ti₃GeC₂) without He clusters is 2.79 J m⁻² (or 2.40 J m⁻²), which is in good agreement with the value, 2.82 J m⁻², reported in ref. 26. However, the value keeps decreasing with the increase in size of He cluster in the A layer and reduces to 37.22% (or 38.13%) of the perfect materials.

Although the He damage for Ti₃GeC₂ is similar to that for Ti₃SiC₂, the latter should be a better candidate as a nuclear structural material because its ideal tensile strength σ_M and maximum strain ϵ_M are always clearly higher than that of the former in the presence (or absence) of the He clusters. In addition, the high mobility of a single He atom in the Si layer with only 0.05 eV diffusion barrier, which is significantly smaller than the value of 0.36 eV in the Ge layer, is beneficial for the He atoms to migrate quickly to the grain boundary.

4. Conclusion

Using DFT calculations, we systematically investigated the effects of He clusters formed in Ti₃AC₂ (A = Ge, Si) on the mechanical properties and obtained the following conclusions. First, the interstitial He atoms homogeneously generated in Ti₃AC₂ would immediately ($\sim 10^{-6}$ s) migrate to the A layer at higher temperature (>500 °C) and form clusters of no more than 7 He atoms at a mono-vacancy in the A layer. Second, the cluster of V-7He atoms severely reduces the ideal tensile strength, 31.93 GPa, of Ti₃SiC₂ (or 26.56 GPa of Ti₃GeC₂) to 11.90 GPa (or 9.42 GPa), and the corresponding maximum strain changes from 0.19 (or 0.17) to 0.08 (or 0.07), showing heavy damage effects on the mechanical properties. Third, the strain simulations showed that the fracture of Ti₃AC₂ would mostly occur around the A layer with the presence (or absence) of the He clusters, whereas Ti₃C₂ blocks are relatively stable, and the embrittlement was enhanced with the increase in He cluster size. At last, we conclude that as nuclear structural materials, Ti₃SiC₂ should be better than Ti₃GeC₂.

Conflicts of interest

There are no conflicts to declare.

Acknowledgements

This study was supported by the National Natural Science Foundation of China [Grant No. 11274073 and No. 61675045].

References

- 1 H. Trinkaus and B. N. Singh, *J. Nucl. Mater.*, 2003, **323**, 229–242.
- 2 E. A. Marquis, J. M. Hyde, D. W. Saxey, S. Lozano-Perez, V. de Castro, D. Hudson, C. A. Williams, S. Humphry-Baker and G. D. W. Smith, *Mater. Today*, 2009, **12**, 30–37.
- 3 I. J. Beyerlein, A. Caro, M. J. Demkowicz, N. A. Mara, A. Misra and B. P. Uberuaga, *Mater. Today*, 2013, **16**, 443–449.
- 4 M. J. Caturla, T. D. de la Rubia and M. Fluss, *J. Nucl. Mater.*, 2003, **323**, 163–168.
- 5 W. D. Wilson, C. L. Bisson and M. I. Baskes, *Phys. Rev. B*, 1981, **24**, 5616–5624.
- 6 D. W. Clark, S. J. Zinkle, M. K. Patel and C. M. Parish, *Acta Mater.*, 2016, **105**, 130–146.
- 7 D. J. Tallman, L. F. He, B. L. Garcia-Diaz, E. N. Hoffman, G. Kohse, R. L. Sindelar and M. W. Barsoum, *J. Nucl. Mater.*, 2016, **468**, 194–206.
- 8 H. F. Zhang, B. D. Yao, L. Q. Shi, D. J. O'Connor, J. Huang, J. Y. Zhang, W. Ding and Y. X. Wang, *Acta Mater.*, 2015, **97**, 50–57.
- 9 H. H. Shen, F. Z. Li, H. B. Zhang, S. M. Peng, X. T. Zu and K. Sun, *J. Eur. Ceram. Soc.*, 2017, **37**, 855–858.
- 10 P. Song, J. Sun, Z. Wang, M. Cui, T. Shen, Y. Li, L. Pang, Y. Zhu, Q. Huang and J. Lü, *Nucl. Instrum. Methods Phys. Res., Sect. B*, 2014, **326**, 332–336.
- 11 C. Wang, T. Yang, S. Kong, J. Xiao, J. Xue, Q. Wang, C. Hu, Q. Huang and Y. Wang, *J. Nucl. Mater.*, 2013, **440**, 606–611.
- 12 M. K. Patel, D. J. Tallman, J. A. Valdez, J. Aguiar, O. Anderoglu, M. Tang, J. Griggs, E. G. Fu, Y. Q. Wang and M. W. Barsoum, *Scr. Mater.*, 2014, **77**, 1–4.



- 13 J. R. Xiao, C. X. Wang, T. F. Yang, S. Y. Kong, J. M. Xue and Y. G. Wang, *Nucl. Instrum. Methods Phys. Res., Sect. B*, 2013, **304**, 27–31.
- 14 L. X. Jia, Y. X. Wang, X. D. Ou, L. Q. Shi and W. Ding, *Mater. Lett.*, 2012, **83**, 23–26.
- 15 S. Yang, N. Hu, X. Gou, C. Wang, X. Zhu, W. Duan and L. Yang, *RSC Adv.*, 2016, **6**, 59875–59881.
- 16 Q. Song, P. Zhang, J. Zhuang and X.-J. Ning, *Comput. Mater. Sci.*, 2017, **137**, 327–331.
- 17 Z. F. Zhang, Z. M. Sun and H. Hashimoto, *Mater. Lett.*, 2003, **57**, 1295–1299.
- 18 B. J. Kooi, R. J. Poppen, N. J. M. Carvalho, J. T. M. De Hosson and M. W. Barsoum, *Acta Mater.*, 2003, **51**, 2859–2872.
- 19 T. Zhen, M. W. Barsoum, S. R. Kalidindi, M. Radovic, Z. M. Sun and T. El-Raghy, *Acta Mater.*, 2005, **53**, 4963–4973.
- 20 K. Morishita, R. Sugano and B. D. Wirth, *J. Nucl. Mater.*, 2003, **323**, 243–250.
- 21 L. Yang, X. T. Zu and F. Gao, *Phys. B*, 2008, **403**, 2719–2724.
- 22 P. E. Blochl, *Phys. Rev. B*, 1994, **50**, 17953–17979.
- 23 J. P. Perdew, J. A. Chevary, S. H. Vosko, K. A. Jackson, M. R. Pederson, D. J. Singh and C. Fiolhais, *Phys. Rev. B*, 1992, **46**, 6671–6687.
- 24 H. J. Monkhorst and J. D. Pack, *Phys. Rev. B*, 1976, **13**, 5188–5192.
- 25 G. Henkelman, B. P. Uberuaga and H. Jónsson, *J. Chem. Phys.*, 2000, **113**, 9901–9904.
- 26 N. I. Medvedeva and A. J. Freeman, *Scr. Mater.*, 2008, **58**, 671–674.
- 27 A. Ganguly, T. Zhen and M. W. Barsoum, *J. Alloys Compd.*, 2004, **376**, 287–295.
- 28 C. Hartsuijker and J. W. Welleman, *Engineering Mechanics*, Springer, Netherlands, 2007.
- 29 Z. M. Sun, *Int. Mater. Rev.*, 2011, **56**, 143–166.
- 30 M. W. Barsoum, *Prog. Solid State Chem.*, 2000, **28**, 201–281.
- 31 H. Z. Zhang and S. Q. Wang, *Acta Mater.*, 2007, **55**, 4645–4655.

